Nanoscale

PAPER

View Article Online
View Journal | View Issue

Cite this: *Nanoscale*, 2014, **6**, 13028

Confocal absorption spectral imaging of MoS_2: optical transitions depending on the atomic thickness of intrinsic and chemically doped MoS_2†

Krishna P. Dhakal,[a,b] Dinh Loc Duong,[a] Jubok Lee,[a,b] Honggi Nam,[a] Minsu Kim,[a] Min Kan,[a,c] Young Hee Lee[a,b] and Jeongyong Kim*[a,b]

Received 3rd July 2014,
Accepted 1st September 2014

DOI: 10.1039/c4nr03703k

www.rsc.org/nanoscale

We performed a nanoscale confocal absorption spectral imaging to obtain the full absorption spectra (over the range 1.5–3.2 eV) within regions having different numbers of layers and studied the variation of optical transition depending on the atomic thickness of the MoS_2 film. Three distinct absorption bands corresponding to A and B excitons and a high-energy background (BG) peak at 2.84 eV displayed a gradual redshift as the MoS_2 film thickness increased from the monolayer, to the bilayer, to the bulk MoS_2 and this shift was attributed to the reduction of the gap energy in the Brillouin zone at the K-point as the atomic thickness increased. We also performed n-type chemical doping of MoS_2 films using reduced benzyl viologen (BV) and the confocal absorption spectra modified by the doping showed a strong dependence on the atomic thickness: A and B exciton peaks were greatly quenched in the monolayer MoS_2 while much less effect was shown in larger thickness and the BG peak either showed very small quenching for 1 L MoS_2 or remained constant for larger thicknesses. Our results indicate that confocal absorption spectral imaging can provide comprehensive information on optical transitions of microscopic size intrinsic and doped two-dimensional layered materials.

Introduction

Molybdenum disulfide (MoS_2) is an emerging two-dimensional layered material that undergoes a distinct transition from a structure that features an indirect bandgap to a structure that features a direct bandgap as the material thins down to a monolayer which suggests promising optoelectronic applications.[1–6] Optical experimental studies of MoS_2 have reported distinct photoluminescence (PL) bands at around 1.9 eV which were attributed to bandgap transition in the K-point of the Brillouin zone.[1,5,7] Studies have also shown that the valence band (VB) is split at the K-point, due to spin–orbit coupling (SOC) (in the monolayer) and also the interlayer interaction energy (in multi-layers) which produces two separate exciton bands, the A and B excitons.[1,5,6] Experimental absorption spectra have shown the A and B exciton transitions at the same energy positions observed in PL measurements.[1,4,8]

However, some recent theoretical studies of the band structure and optical transition spectra of MoS_2 have suggested that monolayer MoS_2 possesses a much larger bandgap and exciton binding energy as well as the existence of an additional absorption peak at around 2.8 eV.[9–14] For example, Cheiwchan-chamnangij *et al.* used the quasiparticle self-consistent GW method which resulted in ~2.75 eV bandgap of monolayer MoS_2,[9] and Molina-S'anchez *et al.* and Qiu *et al.* independently reported the presence of additional high-energy exciton peaks beyond 2.4 eV in the calculated optical spectra using the Bethe–Salpeter equation.[10,11] The time decay and low temperature dependence of the MoS_2 PL excitons were studied, revealing a very fast decay rate of a few ps.[15] Zhang *et al.*[16] reported the use of scanning tunneling spectroscopy and measured a 220 meV exciton binding energy in monolayer MoS_2, much lower than the value predicted by most theoretical calculations.[9–13]

The band structures of MoS_2, particularly the band gap energy at the K-point and the exciton energy level, have not been elucidated, even though extensive theoretical and experi-

[a]*Center for Integrated Nanostructure Physics, Institute for Basic Science (IBS), Suwon 440-746, Korea. E-mail: j.kim@skku.edu; Fax: +82-(0)31-299-6505; Tel: +82-(0)31-299-4054*
[b]*Department of Energy Science, Sungkyunkwan University, Suwon 440-746, Korea*
[c]*Department of Materials Science and Engineering, Peking University, Beijing 100871, China*

† Electronic supplementary information (ESI) available: Details about the confocal scanning spectral imaging system used to obtain the correlated PL, Raman, and absorption spectra and the atomic force microscopy (AFM) results are given. Additional absorption spectra obtained from the monolayer, bilayer, and bulk MoS_2 samples support the consistency of our measurements. Schematic of BV doping, Fourier transform infrared (FT-IR) spectra of MoS_2 films with and without BV doping, decomposition analysis of PL peak and the comparison of confocal absorption spectra with and without the compensation of the wavelength dispersion of the refractive index of the glass substrate are given. See DOI: 10.1039/c4nr03703k

mental studies have been applied toward these aims. The optical absorption spectra of MoS_2 films beyond 2.4 eV can provide critical information about the band structures of MoS_2 and their evolution as a function of the atomic thickness: monolayer, bi-layer, and bulk. Previous reports of optical spectra of the MoS_2 films beyond 2.4 eV lack detailed interpretation about the high-energy absorption peaks and the layer dependence of these peaks were never addressed.[1,17–19] Recently, photoluminescence excitation measurements of mono- and bi-layer MoS_2 were conducted.[20] The absorption peak at ~2.8 eV was attributed to a transition among the nesting bands between the Γ and Λ positions of the Brillouin zone.[21,22]

Doping of two-dimensional transition metal dichalcogenide (TMD) materials exhibits intriguing electronic, optical, structural, and chemical properties that are potentially useful in many optoelectronic devices.[23–28] The monolayer MoS_2 film was doped in various ways by applying gate bias voltage to the MoS_2FET devices, using physisorption gas molecules and chemical solutions.[23–26,28] Chemical doping to the MoS_2 has received special attention, because this way of doping was shown to achieve n-type doping to the degenerate level for few layers of MoS_2 and WS_2 using alkali metal vapor (K vapour),[26] however alkali metals are not stable in an ambient environment which limits their practical applications. Reduced benzyl viologen (BV) possesses high reduction potential values and is regarded as an excellent air stable n-type dopant of the two-dimensional materials.[28–30] Modification of PL and absorption spectra of the doped monolayer MoS_2 showed the formation of the tightly bound trion at high electron concentrations.[23,24] All these optical studies of doped MoS_2 were performed within the spectral range 1.7–2.2 eV, mainly focusing on A and B exciton PL and absorption peaks. Previously, optical spectra of the doped graphene and two-dimensional semiconductor systems were studied and the quenching or enhancement and the spectral shift of PL or absorption peaks were observed.[23,31–34] However, so far no study of optical absorption spectra of the chemically doped MoS_2 film was reported.

We employed solution-based chemical doping using the BV to the various atomic thicknesses of MoS_2 films to achieve the n-type doping effect. BV has been used as an efficient n-type dopant to the CNT and graphene[29,30] and recently was demonstrated on the trilayer MoS_2 film.[28] Here, we investigated the doping effect on PL, absorption and Raman spectra of MoS_2 films with different atomic thicknesses. Optical absorption spectral measurements in two-dimensional materials usually require large-area samples and suffer from low signal of differential reflectance if used on microscopic-sized samples, thereby hindering the systematic study of optical transitions in MoS_2 samples having different atomic thicknesses. Recently, confocal absorption mapping techniques revealed the anisotropic absorption properties of organic single rubrene nanoplates and Au/rubrene hybrid nanofibers.[35,36] Here we describe the absorption spectra of intrinsic and doped MoS_2 thin films having different atomic thicknesses over the range from 1.5 to 3.2 eV using confocal absorption spectral mapping techniques combined with correlated PL, Raman, and AFM measurements.[35] The three distinct absorption bands obtained from each intrinsic and chemically doped MoS_2 film revealed the systematic variations of the peak position and the intensity as the film thickness increases from the monolayer, to the bilayer, to the bulk.

Experimental

Commercial natural 2*H*-MoS_2 crystals (2D Semiconductor Supplies Corp.) were mechanically cleaved using the scotch tape method and were deposited onto a clean transparent slide glass of 1 mm thickness. Apparently thinner regions were located using an optical microscope and then exact film thicknesses were confirmed by the subsequent PL and Raman spectral imaging studies and the AFM imaging results obtained in the same region. The diameter of the illumination volume at the focus for PL and Raman measurements was around 300 nm. Scattered light was collected through the objective used for illumination and was guided to a 30 cm long monochromator (equipped with a cooled CCD) through an optical fiber with a 50 μm core diameter, which acted as a confocal detection pinhole. Diffraction gratings with 150 grooves mm^{-1} and 1200 grooves mm^{-1} were used to collect the PL and Raman spectra, respectively. The 514, 488 and 458 nm lines of an Ar ion laser were used at intensities of less than 500 μW in a lab-made laser confocal microscope system equipped with a 0.95 NA objective lens. With this power level of laser illumination, no physical damage or oxidation is expected to occur on the MoS_2 films.[37] Confocal absorption spectral imaging was used to obtain the local spectra at each scanning pixel position. A schematic diagram of the confocal system used to obtain the correlated spectroscopic measurements of the PL, Raman, and absorption spectra is shown in ESI (Fig. S1†).

We purchased positively charged 1,1′-dibenzyl-4,4′-bipyridinium dichloride (BV^{2+}) (Fluka Chemical Corp.) and reduced it to the neutral benzyl BV using sodium borohydride following the known procedure.[29,30] Solution-based chemical doping was performed using a drop-cast method. The concentration of the BV in toluene solution was 5 mM. An approximately 10 μL droplet of the solution was dispensed using a pipette directly on the sample where the flakes of different thicknesses of MoS_2 films were prepared. All optical measurements were performed after evaporating the solvent under ambient conditions.

Results and discussion

Correlated PL and Raman spectral mapping of the MoS_2 films

Fig. 1 shows the PL and Raman mapping images of a single area of the exfoliated MoS_2 films. This area contained MoS_2 films having a variety of thicknesses, as shown in the optical photograph inset of Fig. 1(b). This area was divided into two regions to collect the absorption, PL, and Raman spectra.

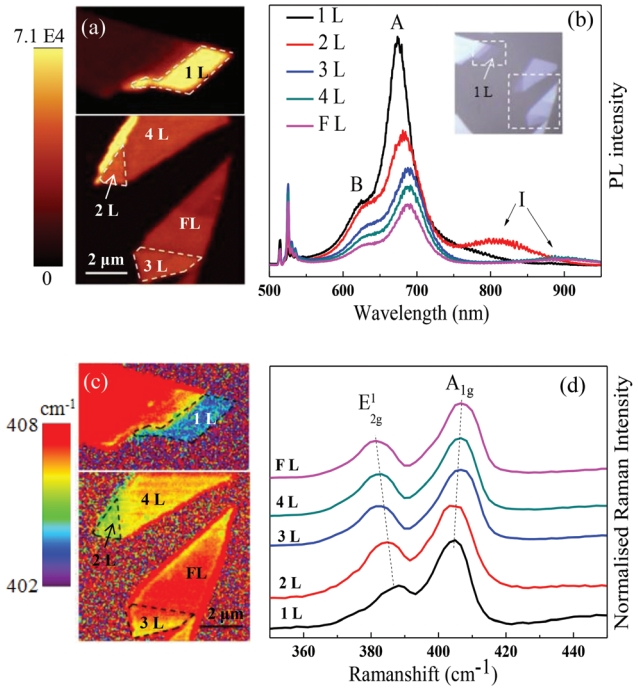

Fig. 1 PL and Raman spectral characterization of the MoS_2 films obtained using 514 nm laser excitation. (a) PL mapping image, showing the integrated intensities of the A and B exciton peaks. The number of layers of MoS_2 films in the mapping area was determined based on the PL intensity, Raman peak positions and AFM measurement. (b) The average PL spectra of the 1L, 2L, 3L, 4L, and FL MoS_2. (c) Raman mapping image that shows the local A_{1g} peak frequency positions. The peak position changes from 404 cm^{-1} for the 1L to 408 cm^{-1} for the FL region. (d) Average Raman spectra obtained from 1L, 2L, 3L, 4L, and FL MoS_2 regions. Lines along the peaks are guides for the eyes.

The boundaries of these regions are indicated with white dotted lines. Fig. 1(a) shows the PL intensity-integrated map, and the averaged PL spectra obtained from each region are plotted in Fig. 1(b). The direct bandgap of the monolayer MoS_2 produced the strongest PL in this sample. The PL intensity decreased with increasing atomic thickness due to the direct-to-indirect bandgap transition. The average PL spectra obtained from each film thickness region displayed this trend, as shown in Fig. 1(b). Two exciton PL peaks at 1.83 eV and 1.98 eV originated from the transition in the K-point of the Brillouin zone.[1,7]

Fig. 1(c) shows the Raman frequency map, and the averaged Raman spectra obtained from each region are plotted in Fig. 1(d). The MoS_2 films showed Raman band positions that depended on the layer number and could be used to identify the MoS_2 layer number.[1,7,19,37–40] Consistent peak positions and a shift in the in-plane (E_{2g}^1) and out-of-plane (A_{1g}) Raman modes of the vibrations in each MoS_2 were observed.[1,37–40] The wave number difference between the E_{2g}^1 and A_{1g} peaks in the Raman spectra has frequently been used to identify the number of MoS_2 layers because these values change with the layer number.[37–40] The PL, Raman, and AFM measurements (ESI, Fig. S2†) were used here to identify the monolayer (1L), bilayer (2L), trilayer (3L), quadruple-layer (4L), and few-layer (FL) regions, as noted in each mapping image. The maps of the A_{1g} Raman band position are displayed in Fig. 1(c) which shows a gradual blue shift in the A_{1g} peak from 404 cm^{-1} to 408 cm^{-1} with increasing film thicknesses. The contrast that appeared in the Raman mapping image is in very good agreement with the original assignment of the layer number. The average Raman spectra obtained from each layer also displayed this trend, as shown in Fig. 1(d).

Confocal absorption spectral imaging of MoS_2

Fig. 2 shows the absorption spectral maps obtained from the regions that had been mapped using PL and Raman spectroscopy. The absorption spectral mappings were carried out using confocal spectral mapping techniques[23] in the reflection mode and covered the spectral range 1.5–3.2 eV. The reflections of the thin absorbing film prepared on a glass substrate are directly proportional to the absorption properties of the film, according to the following relation,[41,42]

$$\frac{\Delta R}{R} = \frac{4}{n_s{}^2 - 1}\alpha(\lambda)n \qquad (1)$$

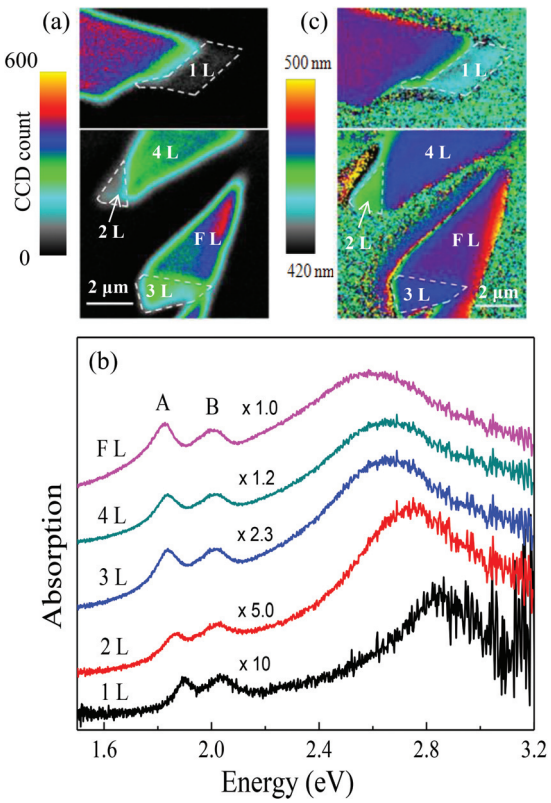

Fig. 2 (a) Absorption spectral mapping image showing the integrated absorption intensities. Each layer represented in the PL and Raman measurements was identified in the absorption mapping study. (b) The peak position mapping of the high-energy absorption peak. The 1L, 2L, and FL regions could be clearly resolved, suggesting that each film thickness provided a constant high-energy absorption peak position. (c) Averaged absorption spectra obtained from each layer. Spectra were normalized by the specified factor and were translated vertically to facilitate the comparison.

where, R, α, n, and n_s represent the measured reflectance, absorption coefficient, refractive index of the film, and refractive index of the substrate, respectively. We assumed n and n_s to be constant and wavelength independent for the spectral range investigated. (See Fig. S9 in ESI† for the comparison of absorption spectra with and without considering the dispersion of refractive index of the glass substrate.) Thus, experimentally measured $\Delta R/R$ was directly proportional to the α and thus, the differential reflection spectra obtained from different atomic thickness regions were regarded as the measure of the absorption spectra. All the absorption spectra were collected under identical illumination intensities and exposure times. The total integrated absorption intensity mappings of the same sample regions are displayed in Fig. 2(a). The regions identified as having different atomic thicknesses are indicated. These regions displayed uniform absorption strength throughout, except at the boundaries between regions having different thicknesses due to the finite (~1 μm) spatial resolution of the confocal absorption mapping. The absorption intensity increased with the atomic thickness. Interestingly, the absorption strength of 2L was almost exactly twice that of 1L; however, this proportionality constant did not hold beyond 3L.

Fig. 2(b) shows representative absorption spectra obtained from each layer region. The spectra were enlarged by certain factors and given offsets to facilitate a comparison. Three main features appeared in the absorption spectrum as A and B exciton peaks embedded in a continuous spectrum, with a maximum peak near 2.84 eV in the monolayer MoS_2. The 1L region provided 1.88 eV and 2.03 eV peaks for the A and B exciton positions, similar to the values observed in the PL spectra in Fig. 1. The splitting energy between the A and B peaks amounted to 0.15 eV in the monolayer and increased with increasing MoS_2 film thickness, reaching 0.16 eV in the bilayer and 0.19 eV in the bulk. This splitting caused by the splitting in VB is mostly due to SOC and some interlayer coupling present in the multilayer MoS_2 film.[1,9] This trend of increasing splitting energy was also observed in the APRES study on $MoSe_2$[43] and the theoretical calculations for MoS_2 are summarized in Table 1. Interestingly, only the A exciton band displayed a clear redshift with increasing thickness, discussed further below.

Table 1 Peak positions of the absorption bands of the A exciton, B exciton, and background (BG). The splitting energy between A and B excitons (VBS), observed here in comparison with the values reported previously, is shown. Also shown are the observed shifts in the difference between the A exciton peak and the BG peak (BG shift), and the predicted shift of the band gap energy (E_g shift) as a function of the sample thickness. (All units are eV)

	Monolayer	Bilayer	Trilayer	Bulk
A exciton	1.88	1.86	1.83	1.82
B exciton	2.03	2.02	2.01	2.01
BG[a] peak	2.84	2.73	2.65	2.61
VBS[b] (exp.)	0.15	0.16	0.18	0.19
VBS[b] (ref.)	0.11[c], 0.10[d]	0.16[c]		0.23[c]
BG shift	0	−0.11	−0.19	−0.23
E_g (K-point) shift	0	−0.09[c]		−0.18[c]

[a] Background. [b] Valence band splitting energy. [c] Ref. 10. [d] Ref. 11.

Evolution of the high-energy absorption peak depending on the atomic thickness of MoS_2

A high-energy absorption peak was observed at 2.84 eV in the monolayer, consistent with recent experimental studies[20] and theoretical calculations.[10,11,21] This large background (BG) peak in the absorption spectrum may be understood as a broadening of the high-energy exciton peaks due to phonon–electron coupling.[11] We note that the peak position of this BG absorption peak decreased in energy and the spectral width increased with the film thickness. The peak position of this BG absorption band was closely related to the film thickness, as observed in the mapping images of the BG absorption band, as shown in Fig. 2(c) and, interestingly, very close to the band-edge energy at the K-point predicted in a theoretical study.[11] Each region having a different MoS_2 film thickness co-overlapped with the peak position distribution of the BG absorption band. The high energy absorption peaks have been observed in previous experimental studies of MoS_2; however, the origin of these peaks has not been discussed in detail, and the dependence on the film thickness has not been evaluated.[17,19,20]

The observed absorption spectra and their dependence on the atomic thickness were modeled using a simple band transition scheme to describe the mono-, bi-, and bulk MoS_2 regions, as shown in Fig. 3. The top of the valence band at the K-point was used as a reference in this diagram. It should be noted that the shift of the A exciton peak originated from the change of exciton binding energy or the gap between the lowest conduction band (CB) and the highest valence band at the K-point or a combination of both effects. The B-exciton position did not change significantly because the reduction in the exciton level was offset by an increase in the VB splitting.

A 458 nm wavelength (2.70 eV) laser was used to conduct the PL measurements at the on-resonance excitation of the BG absorption peak. The indirect PL observed under these conditions was much stronger than the PL intensity observed using 514 nm excitation. Fig. 4(a) and 4(b) show the results of the PL mapping study, obtained in this new area using 514 nm (2.41 eV) and 458 nm (2.70 eV) laser excitation, respectively. The peak height of the A exciton band was normalized to reveal a factor of 4.5 increase in the indirect band PL of the bilayer MoS_2 when excited with 2.70 eV (compared to excitation at 2.41 eV). We attribute this increase in the indirect PL band to the relaxation of a larger number of generated carriers to the neighboring indirect band CB valley located between the K- and Γ-point of the Brillouin zone.

We observed that the BG absorption peak at 2.84 eV in 1L MoS_2 shifted gradually as the MoS_2 thickness increased, reaching saturation at 2.61 eV in the bulk MoS_2. It is interesting to see our thickness-dependent shift in the BG peak correlated to the shift predicted theoretically based on bilayer and bulk MoS_2 models, which found that the gap at the K-point

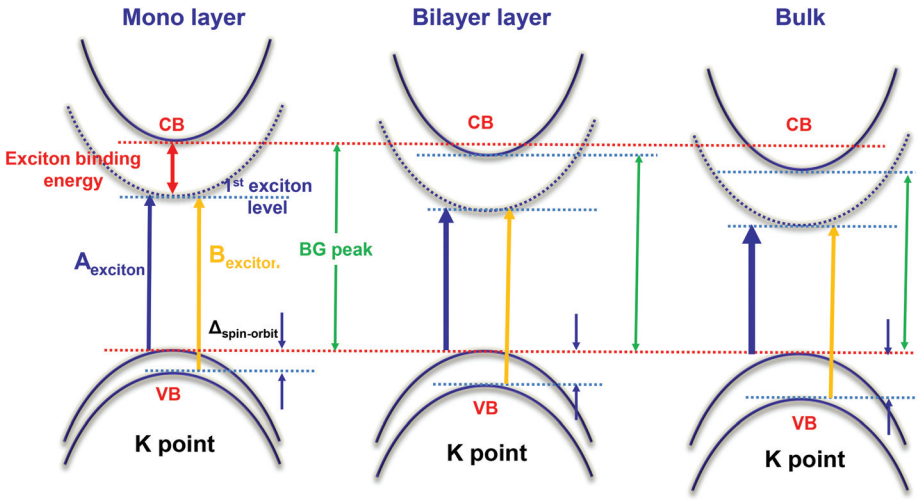

Fig. 3 Schematic diagram showing the optical transition at the K-point in the monolayer, bilayer, and bulk MoS_2 regions. The red shift in the A exciton peak originated from the lowering of the 1st exciton level. The B-exciton peak position did not change significantly because the reduction in the exciton level was offset by an increase in the valence band (VB) splitting energy. The background peak corresponds to the energy difference between the conduction band and the VB.

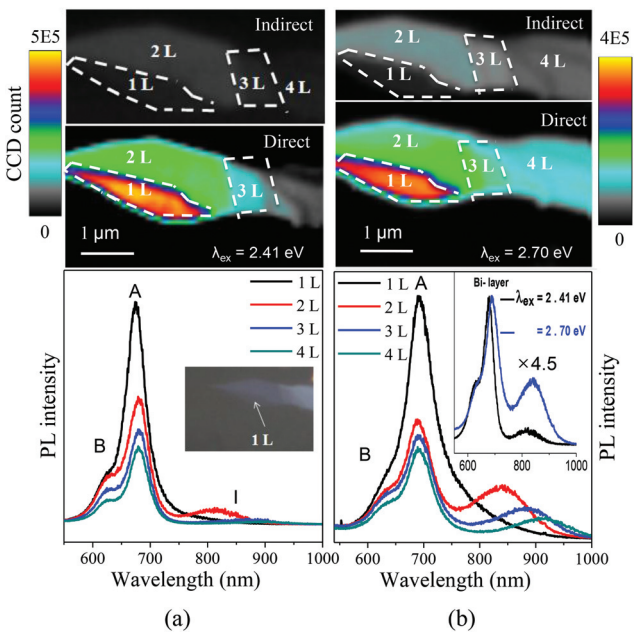

Fig. 4 (a) PL mapping results obtained using 514 nm (2.41 eV) laser excitation. The inset shows the optical microscopy image of the measured area. (b) PL mapping results obtained using 458 nm (2.70 eV) excitation. Note that the indirect PL band of the bilayer at 840 nm (1.48 eV) was much stronger than the intensity obtained using 2.41 eV excitation. The inset shows a comparison of the normalized PL spectra obtained from the two laser excitation wavelengths.

decreased with increasing thickness.[10] The gap reductions of −0.09 eV and −0.18 eV for the bilayer and bulk, respectively, are similar to our observations of the BG peak shifts of 0.09 eV and 0.23 eV, even though this work predicted the bandgap to be 2.2 eV, substantially smaller than the observed BG absorption peaks. Further experiments are required to prove whether this similarity originated from the BG peak that represents the band-edge energy in the K-point or just a coincidental appearance.

Doping effect on the optical properties of the MoS_2

Fig. 5 displays the PL and Raman results of the chemically doped MoS_2 films using BV. This area (the same area shown in the optical photograph of the inset of Fig. 4(a)) contained MoS_2 films having different atomic thicknesses. Fig. 5(a) shows the PL intensity-integrated map, and the averaged PL spectra obtained from each thickness region before and after the doping by BV. The clear quenching and the redshift of the A exciton peak from PL spectra of 1L, 2L and 4L layer MoS_2 films are observed as effects of the doping as shown in Fig. 5(a). We observed a significant reduction and the red shift by 12 nm of the A exciton PL peak in the case of 1L MoS_2, while these spectral modifications of PL on 2L and 4L are smaller. (See the ESI and Fig. S6, S7 and S8† for the decomposition of the PL peak into A, B and "trion" peaks and their variations in peak positions and the relative intensities with BV doping). This less effect of doping on thicker MoS_2 films could be because the BV adsorption mainly occurred on the topmost layer, which is similar to the case of chemically doped multilayer graphenes.[44] The observed spectral modifications of PL spectra as an effect of the BV doping are consistent with previous reports obtained with electrically doped 1L MoS_2 films which are attributed to the quenching phenomena of the neutral exciton peak and the emergence of the trion peak, as the excess electrons are injected to the MoS_2 by the charge transfer phenomena of chemical doping.[23,24] These results showed that our BV treatment successfully performed the n-type doping of the mono- and multi layer MoS_2 films.

Fig. 5(b) shows the map of A_{1g} Raman band position and the average Raman spectra obtained from each thickness

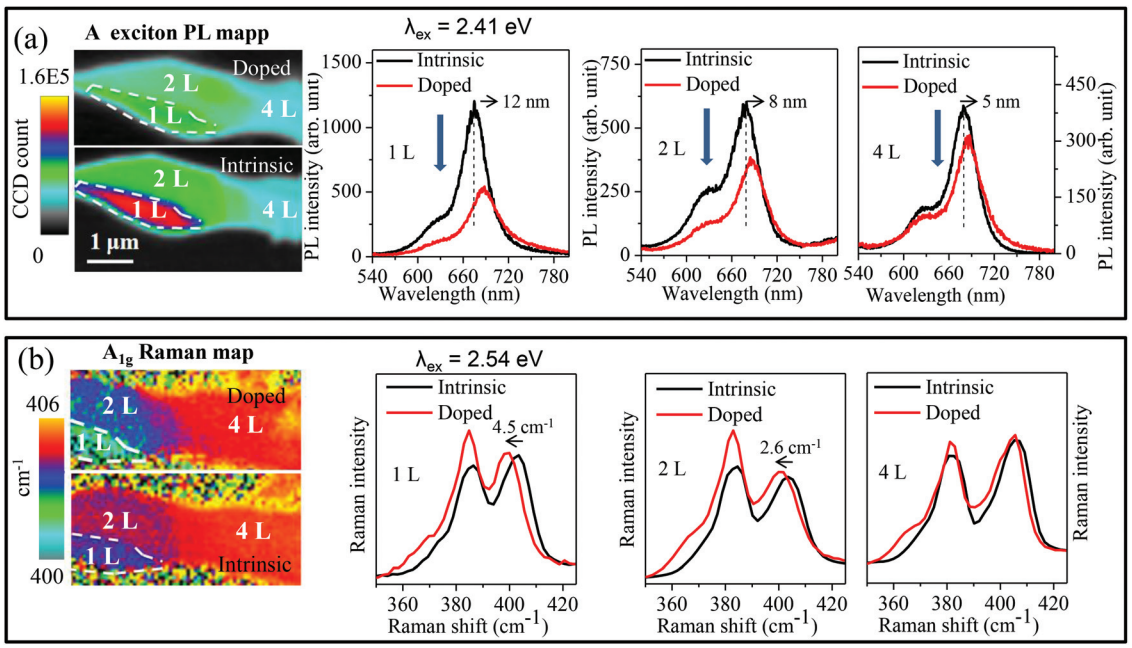

Fig. 5 PL and Raman spectral characterization of the intrinsic and BV doped MoS_2 films. (a) PL mapping image shows the direct comparison of the PL integrated intensities of the A and B exciton peaks obtained from intrinsic and doped MoS_2 films of different thicknesses. The layer number dependent effect of chemical doping is also demonstrated on the average PL spectra of the 1L, 2L and 4L where the dotted line guides the peak position shift that occurred as a result of the doping. (b) Raman mapping image correlated with the A_{1g} peak frequency. The softening of the A_{1g} peak frequency as an effect of doping is noticed. Average Raman spectra from 1L, 2L and 4L demonstrate the direct comparison and layer number dependence of the intrinsic and doped MoS_2 films.

region before (black curve) and after (red curve) the BV chemical doping. Raman spectra of CNT, graphene and MoS_2 have been used to diagnose the doping level, because vibrational energy is renormalized due to the electron–phonon interaction.[25,28–30,45,46] Observed thickness dependent shifts of A_{1g} and $E_{2g}{}^1$ Raman bands are consistent with the previously reported results.[1,7,19,37] As shown in Fig. 5(b), Raman spectra of the BV doped MoS_2 films taken from 1L, 2L and 4L thicknesses showed the softening of the A_{1g} Raman band by 4.5 cm^{-1} for 1L and 2.6 cm^{-1} for 2L and the softening was negligible for the 4L case. The shift of the $E_{2g}{}^1$ Raman band position was much less affected by the doping, where the shift was only 0.82 cm^{-1} in 1L MoS_2 and less in 2L and 4L MoS_2. This is due to the stronger electron–phonon coupling of the A_{1g} mode than the $E_{2g}{}^1$ mode as the MoS_2 films are doped into n-type.[25,28] This thickness dependence of Raman band softening owing to the BV adsorption suggests again that the adsorption of BV molecules mainly occurred on the topmost layer of multilayer samples. However we cannot exclude the possibility that the BV adsorption properties of MoS_2 may change with the film thickness. In either case Raman spectra obtained before and after the BV doping of MoS_2 films confirmed that adsorption of BV molecules on the surface of the 1L and multi layer MoS_2 films (see ESI Fig. S5† for FT-IR signature of BV adsorption on the MoS_2 surface) effectively doped MoS_2 films. We compare the level of our doped 1L MoS_2 with the amount of the A_{1g} band shift in the Raman spectra. According to Chakraborty *et al.*,[25] softening of the A_{1g} band by 4 cm^{-1} corresponded to 1.8×10^{13} cm^{-2} electron sheet density for the monolayer MoS_2. This suggests that the observed 4.5 cm^{-1} decrease of the A_{1g} Raman band with 5 mM BV solution must have provided the similar doping level which is the same order of the electron sheet density of degenerately doped level of a few layer MoS_2 (1.0×10^{13} cm^{-2}) achieved with K vapour.[26] This observation shows that chemical doping by BV is an efficient way of n-type doping for the 1L and multi layer MoS_2 and also suggests that it may be applied for the tuning of electronic structures of other two-dimensional TMD materials.

Fig. 6 shows the absorption spectra of different atomic thickness (1L, 2L and 4L) MoS_2 films before and after chemical doping by BV. Our observation showed the strong quenching of A and B exciton absorption peaks for 1L MoS_2 and less effect for the thicker films. A small amount of the redshift (~30 meV) in the A exciton band was also observed for 1L MoS_2 as highlighted in Fig. 6(b). Recent studies of optical absorption spectra with the gate voltage applied to the monolayer MoS_2 have also shown the reductions and the redshift of the A and B exciton absorption peaks.[23] The effects of chemical doping on the absorption spectra of different atomic thicknesses of MoS_2 are demonstrated here for the first time. We note that the BG absorption peak shows much less effect on the absorption intensity and the peak position, and virtually remains constant in larger thicknesses of MoS_2. This suggests that the nature of the BG peak is different from the A and B

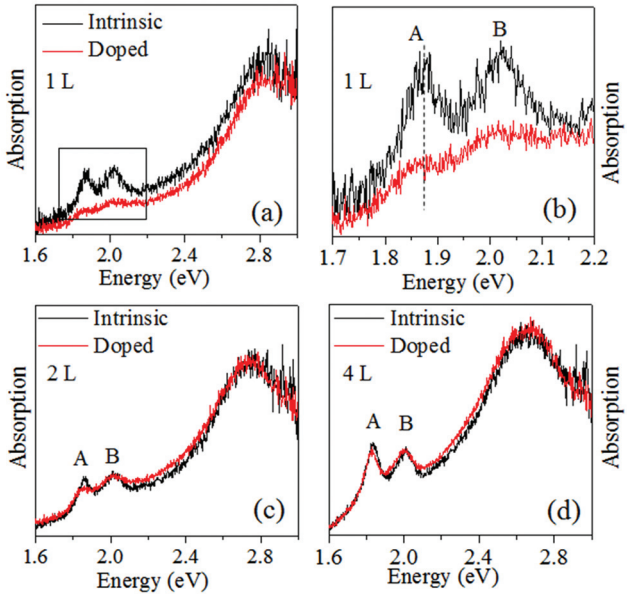

Fig. 6 Absorption spectra of intrinsic (black curve) and chemically doped (red curve) MoS_2 films obtained from the 1L, 2L and 4L. (a) A and B excitons in the monolayer are strongly quenched after doping while the BG peak is much less quenched. (b) Some (~30 meV) redshifts of A and B absorption bands are observed for 1L MoS_2. (c, d). Absorption spectra of intrinsic and chemically doped 2L and 4L MoS_2. Less quenching of A and B peaks is observed with increasing thickness of MoS_2. The BG peak stays constant for 2L and 4L thickness layers.

exciton peaks. The recent photocurrent study result of the monolayer MoS_2, which showed, under a lower bias voltage, A and B excitons were totally quenched while the BG peak maintained its intensity, which was attributed to the unbound nature of the BG peak-corresponding exciton.[47] This report is in good agreement with our observation, because unbound e–h pair is hardly influenced by the increase of excess carrier concentration.[48,49] Further experiments and analysis are required to fully understand the origin of the BG absorption peak.

Conclusions

Full absorption spectra over the range 1.6–3.2 eV were obtained with submicron spatial resolution from intrinsic and chemically doped MoS_2 samples having different atomic thicknesses using confocal absorption spectral imaging. In addition to the characteristic A and B exciton bands observed at 1.88 and 2.03 eV, strong background absorption peaks were observed at 2.84 eV for the monolayer MoS_2 absorption spectra. All absorption peaks displayed gradual red shifts as the atomic thickness increased. The observed absorption spectra and their dependence on the atomic thickness were explained with a simple band scheme and were partially consistent with theoretical predictions and should help to understand the variations of the optical transitions of MoS_2 as a function of the atomic thickness. In addition, we studied the optical transitions of chemically doped MoS_2 using BV and observed that A and B absorption peaks quenched strongly for 1L MoS_2 while the BG absorption peak either showed very small quenching for 1L MoS_2 or remained constant for larger thicknesses.

Acknowledgements

This work was supported by project code (IBS-R011-D1).

Notes and references

1 K. F. Mak, C. Lee, J. Hone, J. Shan and T. F. Heinz, *Phys. Rev. Lett.*, 2010, **105**, 136805.
2 Y. H. Chang, C. T. Lin, T. Y. Chen, C. L. Hsu, Y. H. Lee, W. Zhang, K. H. Wei and L. J. Li, *Adv. Mater.*, 2013, **25**, 756–760.
3 B. Radisavljevic, A. Radenovic, J. Brivio, V. Giacometti and A. Kis, *Nat. Nanotechnol.*, 2011, **6**, 147–150.
4 W. Choi, M. Y. Cho, A. Konar, J. H. Lee, G. Cha, S. C. Hong, S. Kim, J. Kim, D. Jena, J. Joo and S. Kim, *Adv. Mater.*, 2012, **24**, 5832–5836.
5 H. Zeng, J. Dai, W. Yao, D. Xiao and X. Cui, *Nat. Nanotechnol.*, 2012, **7**, 490–493.
6 Z. Y. Zhu, Y. C. Cheng and U. Schwingenschlögl, *Phys. Rev. B: Condens. Matter*, 2011, **84**, 153402.
7 A. Splendiani, L. Sun, Y. Zhang, T. Li, J. Kim, C. Y. Chim, G. Galli and F. Wang, *Nano Lett.*, 2010, **10**, 1271–1275.
8 H. Shi, R. Yan, S. Bertolazzi, J. Brivio, B. Gao, A. Kis, D. Jena, H. G. Xing and L. Huang, *ACS Nano*, 2013, **7**, 1072–1080.
9 T. Cheiwchanchamnangij and W. R. L. Lambrecht, *Phys. Rev. B: Condens. Matter*, 2012, **85**, 205302.
10 A. Molina-S'anchez, D. Sangalli, K. Hummer, A. Marini and L. Wirtz, *Phys. Rev. B: Condens. Matter*, 2013, **88**, 045412.
11 D. Y. Qiu, F. H. da Jornada and S. G. Louie, *Phys. Rev. Lett.*, 2013, **111**, 216805.
12 A. Ramasubramaniam, *Phys. Rev. B: Condens. Matter*, 2012, **86**, 115409.
13 H. Shi, H. Pan, Y.-W. Zhang and B. I. Yakobson, *Phys. Rev. B: Condens. Matter*, 2013, **87**, 155304.
14 H.-P. Komsa and A. V. Krasheninniko, *Phys. Rev. B: Condens. Matter*, 2012, **86**, 241201.
15 T. Korn, S. Heydrich, M. Hirmer, J. Schmutzler and C. Schüller, *Appl. Phys. Lett.*, 2011, **99**, 102109.
16 C. Zhang, A. Johnson, C. L. Hsu, L. J. Li and C. K. Shih, *Nano Lett.*, 2014, **14**, 2443–2447.
17 G. Eda, H. Yamaguchi, D. Voiry, T. Fujita, M. Chen and M. Chhowalla, *Nano Lett.*, 2011, **11**, 5111–5116.
18 L. A. King, W. Zhao, M. Chhowalla, D. J. Rileya and G. Eda, *J. Mater. Chem. A*, 2013, **1**, 8935–8941.
19 Q. Ji, Y. Zhang, T. Gao, Y. Zhang, D. Ma, M. Liu, Y. Chen, X. Qiao, P. H. Tan, M. Kan, J. Feng, Q. Sun and Z. Liu, *Nano Lett.*, 2013, **13**, 3870–3877.

20 D. Kozawa, R. Kumar, A. Carvalho, A. K. Kumar, W. Zhao, S. Wang, M. Toh, R. M. Ribeiro, A. H. C. Neto, K. Matsuda and G. Eda, *Nat. Commun.*, 2014, **5**, 4543.
21 A. Carvalho, R. M. Ribeiro and A. H. C. Neto, *Phys. Rev. B: Condens. Matter*, 2013, **88**, 115205.
22 M. Fox, *Optical properties of solid*, Oxford University Press, Great Clarendon Street, Oxford, OX2 6DP, London, 2007, pp. 66–67.
23 K. F. Mak, K. He, C. Lee, G. H. Lee, J. Hone, T. F. Heinz and J. Shan, *Nat. Mater.*, 2013, **12**, 207–211.
24 S. Mouri, Y. Miyauchi and K. Matsuda, *Nano Lett.*, 2013, **13**, 5944–5948.
25 B. Chakraborty, A. Bera, D. V. S. Muthu, S. Bhowmick, U. V. Waghmare and A. K. Sood, *Phys. Rev. B: Condens. Matter*, 2012, **85**, 161403.
26 H. Fang, M. Tosun, G. Seol, T. C. Chang, K. Takei, J. Guo and A. Javey, *Nano Lett.*, 2013, **13**, 1991–1995.
27 K. Dolui, I. Rungger, C. D. Pemmaraju and S. Sanvito, *Phys. Rev. B: Condens. Matter*, 2013, **88**, 075420.
28 D. Kiriya, M. Tosun, P. Zhao, J. S. Kang and A. Javey, *J. Am. Chem. Soc.*, 2014, **136**, 7853–7856.
29 S. M. Kim, J. H. Jang, K. K. Kim, H. K. Park, J. J. Bae, W. J. Yu, I. H. Lee, G. Kim, D. D. Loc, U. J. Kim, E.-H. Lee, H.-J. Shin, J.-Y. Choi and Y. H. Lee, *J. Am. Chem. Soc.*, 2009, **131**, 327–331.
30 H. -J. Shin, W. M. Choi, D. Choi, G. H. Han, S.-M. Yoon, H.-K. Park, S.-W. Kim, Y. W. Jin, S. Y. Lee, J. M. Kim, J.-Y. Choi and Y. H. Lee, *J. Am. Chem. Soc.*, 2010, **132**, 15603–15609.
31 S. Schmitt-Rink, D. S. Chemla and D. A. B. Miller, *Adv. Phys.*, 1989, **38**, 89–188.
32 E. Burstein, *Phys. Rev.*, 1954, **93**, 632–633.
33 T. S. Moss, *Proc. Phys. Soc. B*, 1954, **67**, 775–782.
34 L. Yang, *Nano Lett.*, 2011, **11**, 3844–3847.
35 H. Lee, J. H. Kim, K. P. Dhakal, J. W. Lee, J. S. Jung, J. Joo and J. Kim, *Appl. Phys. Lett.*, 2012, **101**, 113103.
36 K. P. Dhakal, H. Lee, J. Lee, S. H. Lee, J. Joo and J. Kim, *J. Mater. Chem. C*, 2014, **2**, 1830–1835.
37 H. Li, Q. Zhang, C. C. R. Yap, B. K. Tay, T. H. T. Edwin, A. Olivier and D. Baillargeat, *Adv. Funct. Mater.*, 2012, **22**, 1385–1390.
38 A. G. Bagnall, W. Y. Liang, E. A. Marseglia and B. Welber, *Physica B*, 1980, **99**, 343–346.
39 T. J. Wieting and J. L. Verble, *Phys. Rev. B: Solid State*, 1972, **5**, 1473–1479.
40 C. Lee, H. Yan, L. E. Brus, T. F. Heinz, J. Hone and S. Ryu, *ACS Nano*, 2010, **4**, 2695–2700.
41 J. D. E. Mcintyre and D. E. Aspnes, *Surf. Sci.*, 1971, **24**, 417–434.
42 E. Hecht, *Optics*, Addison-Wesley, Reading, MA, 1998.
43 Y. Zhang, T. Chang, B. Zhou, Y. Cui, H. Yan, Z. Liu, F. Schmitt, J. Lee, R. Moore, Y. Chen, H. Lin, H. Jeng, S. Mo, Z. Hussain, A. Bansil and Z. Shen, *Nat. Nanotechnol.*, 2014, **9**, 111–115.
44 N. Jung, N. Kim, S. Jockusch, N. J. Turro, P. Kim and L. Brus, *Nano Lett.*, 2009, **9**, 4133–4137.
45 A. M. Rao, P. C. Eklund, S. Bandow, A. Thess and R. E. Smalley, *Nature*, 1997, **388**, 257–259.
46 A. Das, S. Pisana, B. Chakraborty, S. Piscanec, S. R. Saha, U. V. Waghmare, R. Yiang, H. R. Krishnamurthy, A. K. Geim, A. C. Ferrari and A. K. Sood, *Nat. Nanotechnol.*, 2008, **3**, 210–215.
47 A. R. Klots, A. K. M. Newaz, B. Wang, D. Prasai, H. Krzyzanowska, D. Caudel, N. J. Ghimire, J. Yan, B. L. Ivanov, K. A. Velizhanin, A. Burger, D. G. Mandrus, N. H. Tolk, S. T. Pantelides and K. I. Bolotin, arXiv:1403.6455 [cond-mat.mes-hall].
48 D. Ninno, F. Liguori, V. Cataudella and G. Iadonisi, *J. Phys.: Condens. Matter.*, 1994, **6**, 9335–9348.
49 T. W. Presist and D. F. Pettengill, *J. Phys. C: Solid State Phys.*, 1973, **5**, 3268–3274.